Separation Science and Technology
Publication details, including instructions for authors and subscription information:
http://www.informaworld.com/smpp/title~content=t713708471

Model Predictions and Experiments for Rotating Reverse Osmosis for Space Mission Water Reuse

Sangho Lee[a]; Richard M. Lueptow[a]
[a] Department of Mechanical Engineering, Northwestern University, Evanston, Illinois, USA

Online publication date: 08 July 2010

To cite this Article Lee, Sangho and Lueptow, Richard M.(2005) 'Model Predictions and Experiments for Rotating Reverse Osmosis for Space Mission Water Reuse', Separation Science and Technology, 39: 3, 539 — 561
To link to this Article: DOI: 10.1081/SS-120027994
URL: http://dx.doi.org/10.1081/SS-120027994

SEPARATION SCIENCE AND TECHNOLOGY
Vol. 39, No. 3, pp. 539–561, 2004

Model Predictions and Experiments for Rotating Reverse Osmosis for Space Mission Water Reuse

Sangho Lee and Richard M. Lueptow*

Department of Mechanical Engineering, Northwestern University, Evanston, Illinois, USA

ABSTRACT

Reverse osmosis (RO) is an efficient process for the removal of ionic and organic pollutants from wastewater. However, flux decline and rejection deterioration due to concentration polarization and membrane fouling hinders the application of RO technology. Rotating RO, which takes advantage of high shear and the Taylor–Couette flow instability to reduce the flux decline related to concentration polarization and membrane fouling, was investigated as a novel method for space mission wastewater recovery. Mass transfer in rotating RO was experimentally determined based on film theory. The model developed for rotating RO allows the prediction of flux and pollutant rejection over a wide range of design and operational parameters. The model matches the experimental

*Correspondence: Dr. Richard M. Lueptow, Department of Mechanical Engineering, Northwestern University, Evanston, IL 60208, USA; Fax: 1-847-491-3915; E-mail: r-lueptow@northwestern.edu.

DOI: 10.1081/SS-120027994 0149-6395 (Print); 1520-5754 (Online)

results from a laboratory-scale rotating RO system very well. According to the model, rotating RO shows better flux and rejection than a non-rotating system by effectively reducing concentration polarization. Operating parameters, such as rotational speed and transmembrane pressure, play an important role in determining the flux and rejection in rotating RO.

Key Words: Reverse osmosis; Rotating filtration; Concentration polarization; Water treatment; Space mission.

INTRODUCTION

For long-term human space flight, recycling of wastewater to produce hygiene and potable water will be necessary to avoid resupply of water and to provide an ongoing safe water supply. However, it is difficult to produce high-quality water from space mission wastewater. The inputs to the wastewater stream include waste hygiene water, condensate water, and urine, each contributing various pollutants that can pose a threat to human health. Although various technologies have been proposed for the recycling of wastewater in space,[1–3] few technologies meet the stringent requirements for space applications.

Among various treatment options, reverse osmosis (RO) is a promising technology for wastewater recovery. Reverse osmosis removes ions and organic chemicals in a stable and predictable manner. Reverse osmosis has been shown to have potential for producing clear water from recycled wastewater in various applications.[4–8] However, concentration polarization and membrane fouling are significant obstacles that limit the acceptance of RO membrane treatment. We considered conventional RO membranes for recycling space mission wastewater[7,8] and found that the potential for membrane fouling is high because of large amounts of inorganic and organic solutes, pathogenic microorganisms, and debris in the wastewater. Therefore, reducing the membrane fouling is of great importance.

Recently, we examined rotating filtration as a new method to minimize concentration polarization and membrane fouling. Rotating filtration takes advantage of high shear and a centrifugal flow instability. The system consists of a cylindrical filter rotating within a concentric cylindrical shell. The flow in the annulus between the filter and shell becomes unstable having toroidal vortical cells, known as Taylor vortices, stacked in the annulus upon exceeding a critical dimensionless rotational speed, $\mathrm{Ta}_c = r_i \omega d/\nu$, the Taylor number, where r_i is the inner cylinder radius, ω is the rotational speed, d is the gap between the inner and outer cylinders, and ν is the kinematic viscosity.

Marcel Dekker, Inc.
270 Madison Avenue, New York, New York 10016

These vortices, which become stronger with increasing Ta, cause a redistribution of the azimuthal momentum in the annulus resulting in a steep velocity gradient at the inner cylinder.[9,10]

Because of its unique hydrodynamics, rotating membrane filtration results in a slower build-up of particles and other species near the filter surface compared to dead-end or crossflow filtration.[11–16] Three mechanisms are responsible for this resistance to fouling in rotating microfiltration: vortices in the annulus between the two cylinders that wash away contaminants from near the filter surface,[17] centrifugal sedimentation of heavy particles away from the filter surface,[18] and shear due to the rotation of the inner cylinder having an effect much like that in crossflow filtration.[15] For rotating RO, similar reductions in concentration polarization have been demonstrated theoretically.[19]

Our model for rotating RO matches experiments quite well for "dynamic dead-end filtration," in which all of the fluid is forced through the RO membrane.[20] While it is helpful to consider dead-end filtration, a rotating RO system will more likely operate with a net flow through the device to carry the concentrated brine out of the system. The focus of this work was to investigate the performance of rotating RO in a through-flow mode rather than dead-end mode under various conditions. We explored the effectiveness of rotating RO in terms of flux and rejection experimentally and theoretically. The long-term goal of our research is to develop a rotating RO water purification and filtration system for use in space.

THEORY

Determination of Mass-Transfer Coefficient

Although many studies have been performed to obtain mass transfer correlations in crossflow membrane modules, no measurements have been made for rotating RO membrane systems, where the rotation of inner cylinder along with Taylor vortices generate high shear. Therefore, we use film theory and Fick's law for diffusion to determine the mass-transfer coefficient in a rotating RO system and its dependence on the Taylor number. The solvent flux, J_v, through the inner cylinder membrane is:

$$J_v = L_v(\Delta P - P_{loss}) \tag{1}$$

where L_v is the solvent transport parameter, ΔP is the pressure difference from the device inlet to the permeate side of the membrane, and $P_{loss} = \Delta\Pi + \Delta P_h$ is the pressure loss by osmotic pressure, $\Delta\Pi$, and hydrodynamic effects in the

MARCEL DEKKER, INC.
270 Madison Avenue, New York, New York 10016

annulus, ΔP_h. The osmotic pressure for a solute i can be calculated by Van't Hoff's equation:[21]

$$\Delta\Pi_i = (C_{m,i} - C_{p,i})RT \tag{2}$$

where $C_{m,i}$ and $C_{p,i}$ are the solute concentrations at the membrane surface on the concentrate side and the permeate side of the membrane, R is the gas constant, and T is temperature. For the conditions considered here, ΔP_h is negligible compared to $\Delta\Pi$.

The solute concentration difference across the membrane, $(C_{m,i} - C_{p,i})$, can be estimated from the pressure difference and water flux by rearranging Eqs. (1) and (2):

$$C_{m,i} - C_{p,i} = \frac{1}{RT}\left(\Delta P - \frac{J_v}{L_v}\right) \tag{3}$$

On the basis of the film model theory and from Fick's law for diffusion, the concentration profile near the membrane surface is:

$$\frac{C_{m,i} - C_{p,i}}{C_{b,i} - C_{p,i}} = e^{J_v/k_i} \tag{4}$$

where $C_{b,i}$ is the solute concentration in the bulk solution and k is the mass-transfer coefficient for the back diffusion of the solute from the membrane to the bulk solution on high pressure side of membrane.[22] Rearranging Eq. (4) using Eq. (3) provides an expression for the mass-transfer coefficient:

$$k_i = \frac{J_v}{\ln((1/RT)(\Delta P - J_v/L_v)/(C_{b,i} - C_{p,i}))} \tag{5}$$

Thus, the mass-transfer coefficient can be found based on a relatively simple experiment where the permeate flux, applied pressure difference, bulk solute concentration, and permeate concentration are measured. This mass-transfer coefficient is then used to predict flux and rejection in rotating RO using the model described below.

Predictive Model for Rotating Reverse Osmosis

The solution-diffusion model modified with the concentration polarization theory was applied to predict rotating RO performance over a wide range of conditions. We only give a broad outline of the model here, since details are provided separately.[19] As shown in Fig. 1, feed solution at pressure ΔP enters the bottom of the annulus between the coaxial porous inner

Marcel Dekker, Inc.
270 Madison Avenue, New York, New York 10016

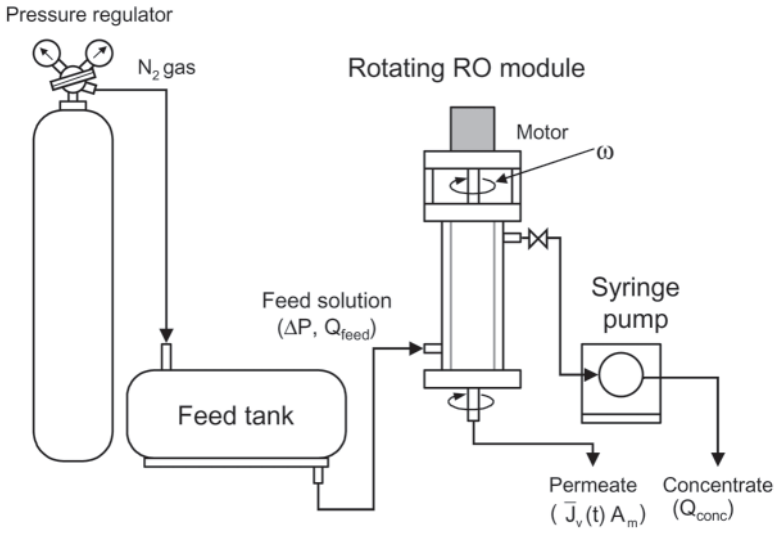

Figure 1. Experimental setup for rotating RO experiments.

cylinder and the outer cylindrical shell at flow rate Q_{feed} and concentration $C_{\text{f},i}$ and travels axially in the annulus. The permeate passes through the porous inner cylinder with flux $J_{\text{v}}(x, t)$ and exits through a hollow shaft at flow rate $\overline{J_{\text{v}}}(t)A_{\text{m}}$, where $\overline{J_{\text{v}}}(t)$ is the flux averaged over membrane area, A_{m}. The concentrate exits at the opposite end of the annulus that it entered at flow rate Q_{conc}. The difference between the concentration of solute i at the membrane, $C_{\text{m},i}$, and its concentration in the bulk solution, $C_{\text{b},i}$, is based on the film model theory and Fick's law for diffusion. The growth of the concentration boundary layer is determined by the mass-transfer coefficient, k_i, as determined using Eq. (5) and measurements.

A mass balance of solute i requires that the time rate of change in $C_{\text{b},i}$ in an annular fluid element is the sum of the change in concentration due to axial flow of solute plus the change in concentration due to the flux of solute through the membrane. The mass balance along with the standard equations for water and solute transport and concentration polarization can be solved for a given geometry (r_{i}, d), rotational speed (ω), transmembrane pressure (ΔP), and flow rate of concentrate out of the device (Q_{conc}). This results in a solution for the flux and solute concentration as functions of time (t) and axial position (x). The average flux through the membrane $\overline{J_{\text{v}}}(t)$ and rejection $R_i\,(t)$ of solute i can be calculated by integrating the local flux and solute concentrations along the length of the filter.

MATERIALS AND METHODS

Figure 1 shows a schematic of the experimental setup for rotating RO. The rotating RO module consisted of a RO membrane rotating within an outer cylindrical housing. A commercially available thin film polymeric RO membrane (Hydranautics, USA) having water permeability of 1.6×10^{-11} m^2 sec/kg (measured using pure water) was bonded to a porous plastic cylindrical support that was mounted on an aluminum support cylinder on a hollow steel shaft. The filter outer radius was $r_i = 2.41$ cm, and the gap width was $d = 0.47$ cm. The length of the filter surface was 12.70 cm, and the overall length of the filter chamber was 23.2 cm. A DC motor permitted rotation of the inner cylindrical RO membrane at rotational speeds ω ranging from 1 to 180 rpm.

Model wastewater was supplied at concentration $C_{f,i}$ from a feed tank pressurized at ΔP into the rotating RO module in the test runs. It entered the annulus between the rotating RO membrane and the outer cylinder at one end of the rotating RO module and traversed axially in the annulus. The permeate flowed through the rotating RO membrane, passed to the center of the hollow shaft through channels within the rotating cylindrical RO membrane unit, and exited the RO module through the end of the hollow shaft. The permeate flux was measured using a graduated cylinder. A syringe pump (Multispeed Transmission, Harvard Apparatus, USA) was used to control the concentrate flow rate, Q_{conc}. The solute concentrations in the concentrate and permeate were measured in several times during the filtration. After each experimental trial, all of the concentrate remaining in the rotating RO module was removed to measure the final solute concentration. The viscosity and density were corrected for temperature, which varied less than 1°C during the experiment.

To determine the mass-transfer coefficient in rotating RO, two different solutions were used: 4000 mg/L of NaCl and 4000 mg/L of Na_2SO_4. All other experiments were performed using a synthetic wastewater that models space mission wastewater, which contains wash water, condensate, and urine. During storage, urea and other organic nitrogen compounds are converted to ammonium ions in the presence of urease from microorganisms in the wastewater,[23] so the wastewater contains ammonium carbonate instead of urea. The composition and properties of the synthetic wastewater used here are summarized in Table 1. In addition to ammonium ions from urine, the wastewater contains NASA body soap and ions.[2] Analysis of ammonium ions was conducted using the procedures described in *Standard Methods*.[24] The spectrophotometric method of Hach[25] was adapted to measure the detergent concentration and chloride ion concentration in the feed, concentrate, and permeate. The total concentration of ions was determined

MARCEL DEKKER, INC.
270 Madison Avenue, New York, New York 10016

Table 1. Composition of simulated space mission wastewater.[7]

Component	Concentration (mg/L)	Total nitrogen (mg/L)
$(NH_4)_2CO_3$	3,429.0	1,000
NASA body soap[a]	190.6[b]	7.8
NaCl	1,000	0

[a]The detergent molecule in NASA body soap is $C_{15}H_{30}O_4NSNa$.
[b]Concentration is based on the net detergent concentration as linear alkylbenzene sulfonate (LAS).

by conductivity measurements, corrected for the influence of temperature. These concentrations were used to calculate the rejection for each solute, i, such that

$$R_i(t) = 1 - \frac{C_{p,i}(t)}{C_{b,i}(t)} \tag{6}$$

where $C_{p,i}(t)$ is the concentration in the permeate and $C_{b,i}(t)$ is the average concentration in the bulk solution calculated based on the inlet and outlet concentrations. The bulk and permeate concentrations were measured several times during each experiment.

To be able to properly apply the model, it is necessary to determine the solute permeability, $L_{s,i}$, for the various solutes. Combining the standard expressions for concentration polarization and solute transport through the membrane, it can be shown that

$$\frac{J_v}{e^{J_v/k_i}} = L_{s,i}\left(\frac{C_{b,i} - C_{p,i}}{C_{p,i}}\right) \tag{7}$$

Thus, the solute permeability, $L_{s,i}$, can be calculated by plotting $J_v/e^{J_v/k_i}$ against $(C_{b,i} - C_{p,i})/C_{p,i}$ for experiments in which J_v, $C_{b,i}$, and $C_{p,i}$ are measured and k_i is based on measurements at different Taylor numbers, as described in the previous section. A set of experiments was performed to obtain $L_{s,i}$ for each solute by varying the transmembrane pressure from 500 to 1000 kPa at $\omega = 90$ rpm using the synthetic wastewater. The average of fluxes and concentrations over the membrane length and over time were used to calculate the solute permeabilities. A commercially available RO membrane (ESPA, Hydranautics, USA) was used for this study. Figure 2 shows the average flux and solute concentrations after 10 min of operation plotted using the format suggested from Eq. (7). From Fig. 2, the solute permeability

MARCEL DEKKER, INC.
270 Madison Avenue, New York, New York 10016

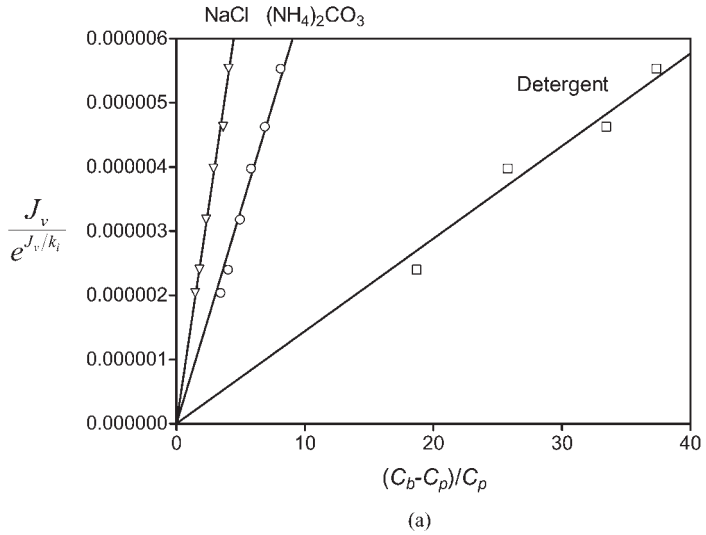

Figure 2. Determination of solute permeability, $L_{s,i}$, based on Eq. (7). The symbols indicate the experimental data and the lines indicate the results of least squares linear fit. $L_{s,i}$ is the slope of the line for each solute. *Key:* ▽, NaCl; ○, $(NH_4)_2CO_3$; □, detergent.

parameters for NaCl, $(NH_4)_2CO_3$, and detergent were 1.3×10^{-6}, 7×10^{-7}, and 1.4×10^{-7} m/sec, respectively.

RESULTS AND DISCUSSION

Mass Transfer in Rotating Reverse Osmosis

The experimental and theoretical results in the literature for measurements of the mass-transfer coefficient for filtration of suspensions in a cylindrical porous rotating cell or the transport of a chemical species in a cylindrical chemical reactor with a nonporous inner cylinder satisfy the relation:

$$\mathrm{Sh} = A\left[\mathrm{Ta}\left(\frac{d}{r_i}\right)^{1/2}\right]^a \mathrm{Sc}^b \tag{8}$$

where $\mathrm{Sh} = 2kd/D$ is the dimensionless mass-transfer rate (Sherwood number), $\mathrm{Sc} = \nu/D$ is the Schmidt number, and D is the diffusion coefficient

of the solute.[16,26] Most previous studies of mass transfer for rotating systems conclude that $A = 0.4–1.1$ and $a = 0.4–0.7$ under vortical flow conditions. Using the analogy between heat and mass transfer, the exponent b for the Schmidt number is assumed to be $1/3$, which has been experimentally confirmed for a large range of Schmidt numbers.[16,27]

In this study, 40 experimental trials, each done in triplicate, were conducted for various transmembrane pressures and rotational speeds. The mass-transfer coefficients were calculated by substituting the measured flux and solute concentrations in the concentrate and the permeate into Eq. (5). Figure 3 shows the dependence of the experimentally measured mass-transfer coefficient, represented as $Sh/Sc^{1/3}$, on the Taylor number. The Sherwood number increases with Taylor number as the rotational shear increases. In addition, the Sherwood number jumps to a higher value at the transition from nonvortical to vortical flow as the vortices redistribute azimuthal momentum, leading to a higher shear and better mass-transfer. The thick solid lines

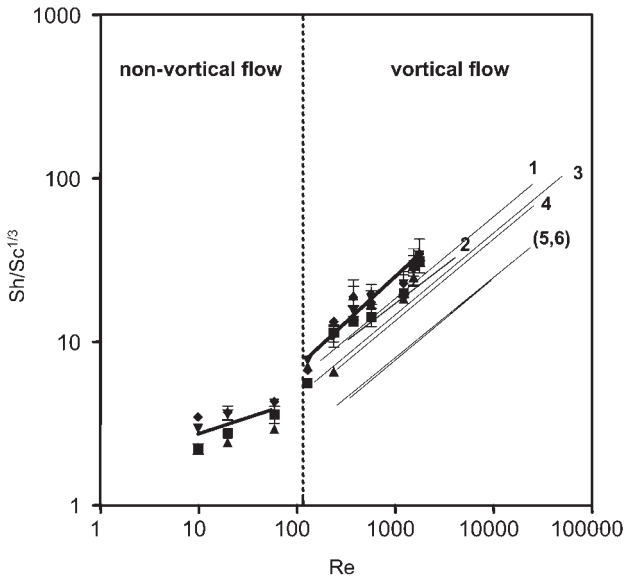

Figure 3. Mass-transfer correlations in rotating RO. Filled symbols indicate the experimental data. Error bars are smaller than the symbol size except in cases where error bars are shown. For vortical flow, thick lines indicate a least squares fit and thin lines indicate the results from previous studies. *Key:* ■, NaCl, 6 atm; ▲, NaCl, 8 atm; ▼, NaCl, 10 atm; ◆, Na_2SO_4, 10 atm. 1. Ref.[16]; 2. Ref.[26]; 3. Ref.[27]; 4. Ref.[30]; 5. Ref.[28]; and 6. Ref.[29].

Marcel Dekker, Inc.
270 Madison Avenue, New York, New York 10016

through the data indicate the least squares fit for each flow regime corresponding to the following equations:

$$\mathrm{Sh} = 2.15\left[\mathrm{Ta}\left(\frac{d}{r_\mathrm{i}}\right)^{1/2}\right]^{0.18}\mathrm{Sc}^{1/3} \quad \text{for nonvortical flow} \tag{9}$$

$$\mathrm{Sh} = 1.05\left[\mathrm{Ta}\left(\frac{d}{r_\mathrm{i}}\right)^{1/2}\right]^{0.51}\mathrm{Sc}^{1/3} \quad \text{for vortical flow} \tag{10}$$

Figure 3 also compares our results with previous studies for vortical flow in rotating filtration and rotating chemical reactors (but not for rotating RO) using various methods, including electrochemical methods for nonporous inner cylinders,[27–29] an ultrafiltration system,[16] a helical-tube analogy,[30] and a theoretical model based on the boundary layer theory.[26] The Sherwood numbers measured for vortical flow in rotating RO are slightly higher than those for other rotating systems, although the trend is consistent with previous measurements. Comparable studies for nonvortical flow are not available to our knowledge, so it is not possible to compare our results to previous studies in this case.

Comparison of Rotating Reverse Osmosis with Nonrotating Reverse Osmosis

Using the synthetic wastewater shown in Table 1, we compare rotating RO with nonrotating RO in terms of permeate flux and solute rejection. The transmembrane pressure was $\Delta P = 1000\,\mathrm{kPa}$ and the concentrate flow rate was $Q_\mathrm{conc} = 0.2\,\mathrm{mL/min}$. Figure 4(a) shows the time-dependent flux $J_\mathrm{v}(t)$ and rejection $R_i(t)$ for nonrotating RO. The symbols are the experimental data and the curves are for the model calculation.[19] The model predicts the flux quite well although the predicted rejection is not as accurate, possibly because $L_{\mathrm{s},i}$ was based on experiments with rotation. Although the pure water flux of the membrane is $57\,\mathrm{L/m^2\,hr}$, the initial permeate flux is less than $15\,\mathrm{L/m^2\,hr}$ because of the high osmotic pressure near the membrane. The flux decreases quickly as filtration proceeds because of the increase in osmotic pressure as solute builds up in the annulus. Although detergent rejection is high, the rejections for ammonium ions and sodium chloride are mediocre.

The flux and rejection for rotating RO under same conditions except that the inner cylinder is rotating at $\omega = 90\,\mathrm{rpm}$ are shown in Fig. 4(b). This rotational speed corresponds to a Taylor number of $\mathrm{Ta} = 1032$, well above the critical Taylor number for the appearance of vortical flow ($\mathrm{Ta/Ta_c} = 9.75$).

Marcel Dekker, Inc.
270 Madison Avenue, New York, New York 10016

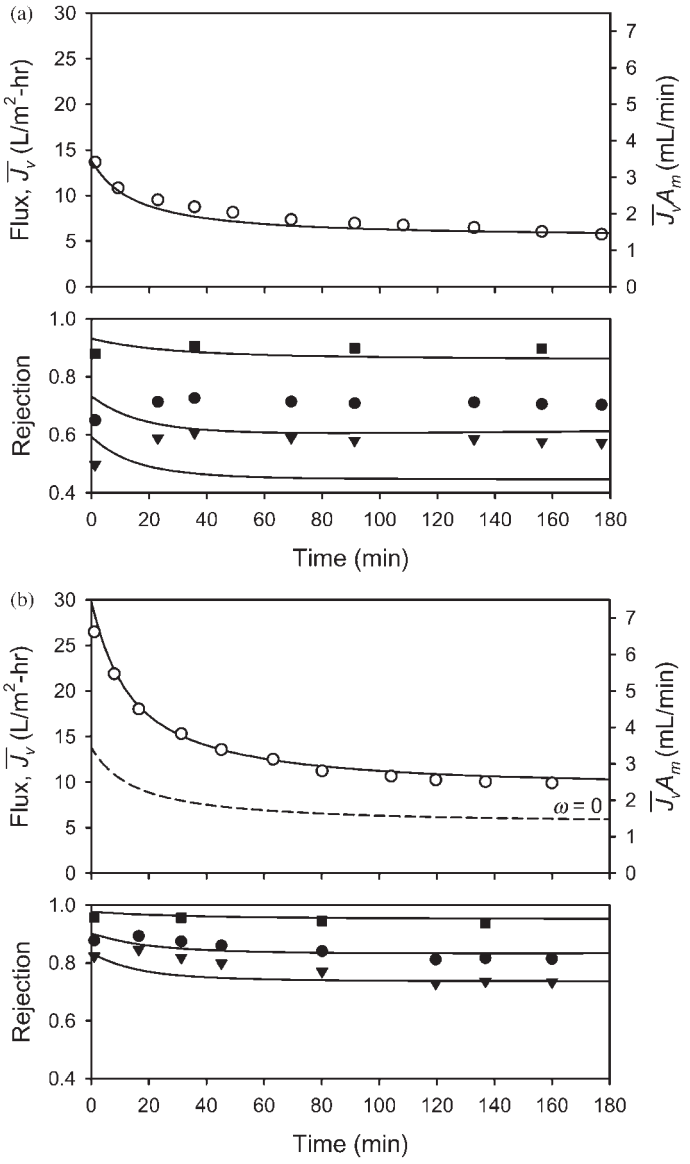

Figure 4. Time dependence of permeate flux and rejection for nonrotating and rotating RO. Condition: $\Delta P = 1000\,\text{kPa}$; $Q_{\text{conc}} = 0.2\,\text{mL/min}$. *Key:* ○, Permeate flux and flow rate; ■, detergent rejection; ●, ammonium carbonate rejection; ▼, NaCl rejection; ——, model. (a) No rotation and (b) $\omega = 90\,\text{rpm}$ ($\text{Ta}/\text{Ta}_c = 9.75$). The dashed line indicates the model flux for no rotation.

In this case, the model matches the experiments quite well. The initial permeate flux is 27 L/m^2 hr, nearly twice than that for nonrotating RO, which is shown as a dashed curve. The flux decreases substantially with time. But even after 180 min, the flux is still 74% higher than that for no rotation. The scale on the right side of the figure helps put this into context. The permeate flow rate after 180 min is $\overline{J_v}A_m = 2.6$ mL/min, while the concentrate flow rate is only $Q_{conc} = 0.2$ mL/min, corresponding to a recovery of 0.92. In addition, the solute rejections for rotating RO are significantly higher than those for nonrotating RO. In particular, the measured NaCl rejection is 28% higher at 160 min for rotation than for nonrotation. This is because the rotation significantly decreases the solute concentration near the membrane. In Fig. 4, the experimental rejection typically rises slightly during the first 30–60 min of operation. We believe that this is a result of the system stabilization. Of course, it is the long-term rejection that is critical for practical applications of rotating RO.

Using our theoretical model, we can compare the solute concentrations in the bulk fluid ($C_{b,i}$) and at membrane surface ($C_{m,i}$) to see the extent of concentration polarization (the ratio of $C_{m,i}$ to $C_{b,i}$) for nonrotating RO and rotating RO. Figure 5 shows $C_{b,i}/C_{f,i}$ and $C_{m,i}/C_{f,i}$ for NaCl, $(NH_4)_2CO_3$, and detergent halfway along the length of the device as a function of time. In case of nonrotating RO, shown in Fig. 5(a), $C_{m,i}/C_{f,i}$ increases very rapidly as solutes build up at the membrane just after $t = 0$. The solute concentrations at the membrane surface remain much higher than those in the bulk solution. On the other hand, the difference between $C_{b,i}/C_{f,i}$ and $C_{m,i}/C_{f,i}$ is much smaller in case of rotating RO, as shown in Fig. 5(b). For example, the concentration polarization ratio for $(NH_4)_2CO_3$ at 180 min is 1.74 for no rotation, while it is only 1.03 for rotating RO. This can be attributed to the enhanced mass transfer in rotating RO system that is related to vortical transport of fluid and a high shear near the membrane. The result is a uniformly high concentration across the entire annular gap rather than a strong concentration polarization layer at the membrane with the consequence being high flux and rejection. Comparing Fig. 5(a) and (b) it is evident that $C_{m,i}/C_{f,i}$ in rotating RO is similar to $C_{m,i}/C_{f,i}$ in nonrotating RO at long times. However, this does not occur because the concentration polarization increases over time but because $C_{b,i}/C_{f,i}$ in rotating RO is much higher than that in nonrotating RO. The consequence is that rotating RO operates at a higher recovery than nonrotating RO.

Influence of Operational Parameters

The effectiveness of rotating RO depends on a wide range of parameters including rotational speed, transmembrane pressure, and flow rate. In Fig. 6,

Marcel Dekker, Inc.
270 Madison Avenue, New York, New York 10016

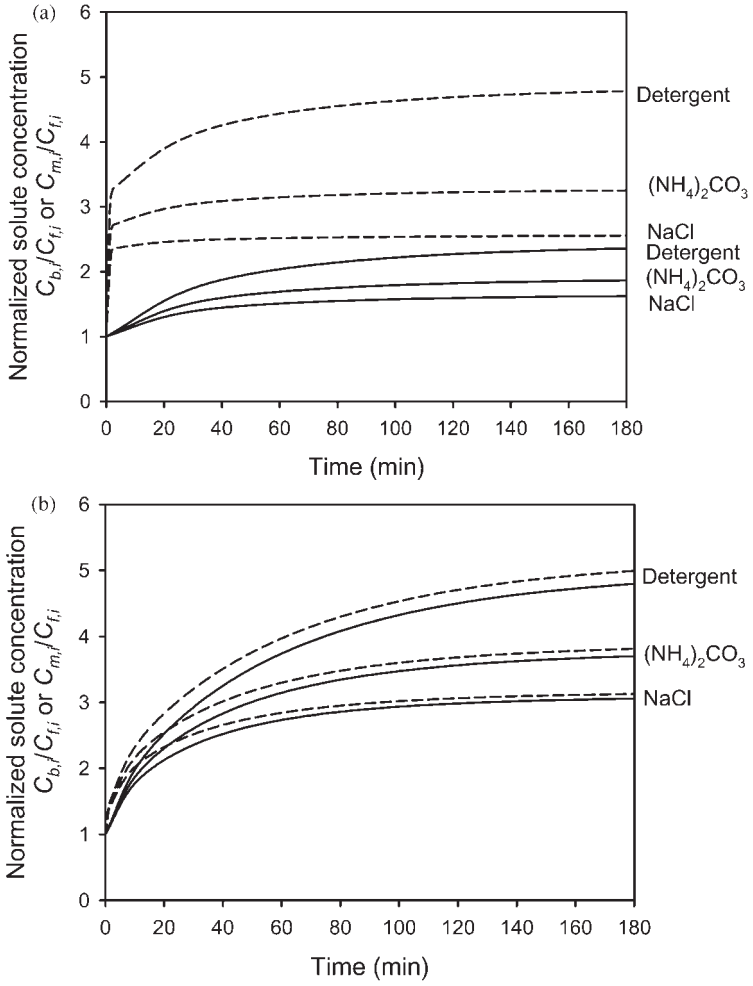

Figure 5. Dependence of C_b and C_m on time at halfway along the length of the device for $\Delta P = 1000\,\text{kPa}$, $Q_{conc} = 0.2\,\text{mL/min}$. *Key:* ——, $C_{b,i}/C_{f,i}$; ------, $C_{m,i}/C_{f,i}$. (a) No rotation and (b) $\omega = 90\,\text{rpm}$ ($\text{Ta}/\text{Ta}_c = 9.75$).

the time dependent variations in flux and total ion rejection are shown for rotational speeds ranging from 7.5 to 180 rpm. We only consider total ion rejection for the remainder of this article, since the rejection for detergent is quite high for all of the experiments. The flux increases as the rotational speed increases with a somewhat larger jump from $\omega = 7.5$ to 15 rpm than between

Marcel Dekker, Inc.
270 Madison Avenue, New York, New York 10016

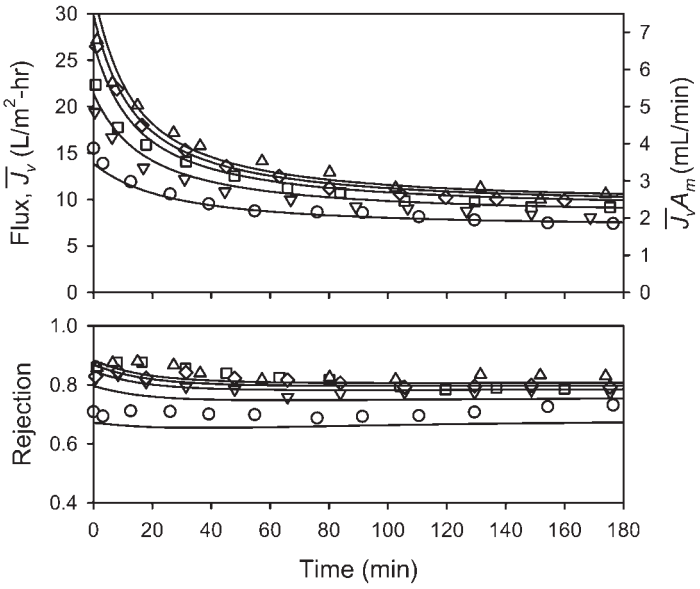

Figure 6. Dependence of permeate flux and total ion rejection on time at various rotational speeds for $\Delta P = 1000\,\text{kPa}$, $Q_{\text{conc}} = 0.2\,\text{mL/min}$. Experiments: ○, $\omega = 7.5\,\text{rpm}$ ($\text{Ta}/\text{Ta}_c = 0.81$); ▽, $\omega = 15\,\text{rpm}$ ($\text{Ta}/\text{Ta}_c = 1.62$); □, $\omega = 45\,\text{rpm}$ ($\text{Ta}/\text{Ta}_c = 4.88$); ◇, $\omega = 90\,\text{rpm}$ ($\text{Ta}/\text{Ta}_c = 9.75$); △, $\omega = 180\,\text{rpm}$ ($\text{Ta}/\text{Ta}_c = 19.5$). Model: ——.

other rotational speeds. This is because the flow transition from nonvortical flow to vortical flow occurs between $\omega = 7.5\,\text{rpm}$ ($\text{Ta}/\text{Ta}_c = 0.81$) and $\omega = 15\,\text{rpm}$ ($\text{Ta}/\text{Ta}_c = 1.62$). Concentration polarization is reduced in the vortical flow regime compared to nonvortical flow because of the enhanced mass-transfer coefficient induced by greater rotational shear and transport due to the vortical motion. No matter what the rotation speed, the permeate flow rate ($\overline{J}_v A_m$) of 1.9–2.7 mL/min is substantially higher than the concentrate flow rate of $Q_{\text{conc}} = 0.2\,\text{mL/min}$, leading to high recovery. The total ion rejection also increases with increasing the rotational speed because of the reduced concentration polarization. The model correctly predicts the trend of experimental data.

Figure 7 illustrates how transmembrane pressure affects permeate flux and rejection in rotating RO. It is evident that flux increases as the transmembrane pressure increases, as would be expected. The increase in rejection with an increased pressure occurs because the solvent flux increases with transmembrane pressure, but the solute flux remains nearly

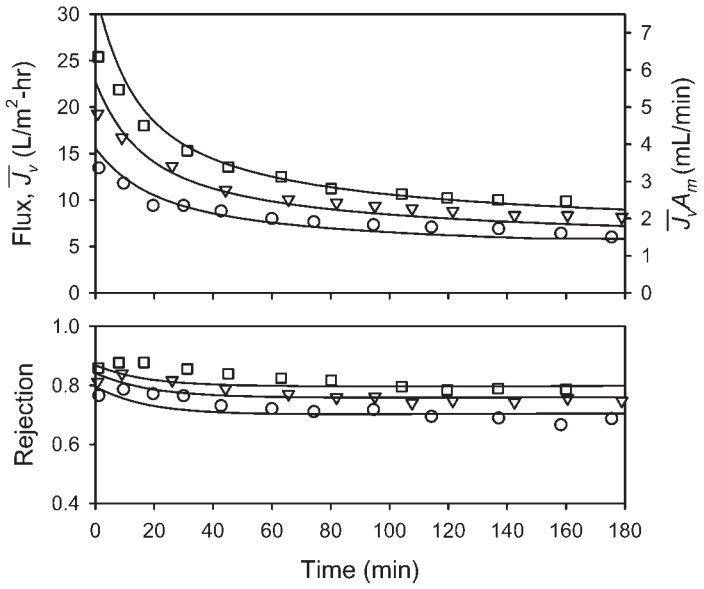

Figure 7. Dependence of permeate flux and total ion rejection on time at various transmembrane pressures for $\omega = 90\,\text{rpm}$ ($\text{Ta}/\text{Ta}_c = 9.75$), $Q_{\text{conc}} = 0.2\,\text{mL/min}$. Experiments: ○, $\Delta P = 600\,\text{kPa}$; ▽, $\Delta P = 800\,\text{kPa}$; □, $\Delta P = 1000\,\text{kPa}$. Model: ——.

constant. The model predicts the effect of the transmembrane pressure on flux quite well.

The concentrate flow rate also affects the recovery in addition to the flux and rejection. Figure 8(a) shows the permeate flux and rejection for concentrate flow rates $0 \le Q_{\text{conc}} \le 1.72\,\text{mL/min}$. Although there are small differences, the model correctly predicts the trends of the experimental data. The flux increases as the waste stream flow (Q_{conc}) increases, because the high flow rate washes solute out of the device. A higher flux results from the lower solute concentration at the membrane. The total ion rejection is nearly independent of Q_{conc}. The rejection at smaller Q_{conc} is slightly lower because the solute build-up in the annulus leads to higher solute transport through the membrane. Figure 8(b) shows the effect of the waste stream flow rate on the recovery, $\overline{J_v}(t)A_m/Q_{\text{feed}}(t)$, where $Q_{\text{feed}}(t) = Q_{\text{conc}} + \overline{J_v}(t)A_m$. As Q_{conc} increases, the recovery decreases because more fluid is washed out of the system instead of being forced through the membrane. Nevertheless, the recovery is quite good for all flow rates. For instance, after 3 hr of operation with $Q_{\text{conc}} = 0.5\,\text{mL/min}$, $\overline{J_v}(t)A_m/Q_{\text{feed}}(t) = 0.86$, corresponding to a permeate flow of $\overline{J_v}(t)A_m = 3.07\,\text{mL/min}$.

MARCEL DEKKER, INC.
270 Madison Avenue, New York, New York 10016

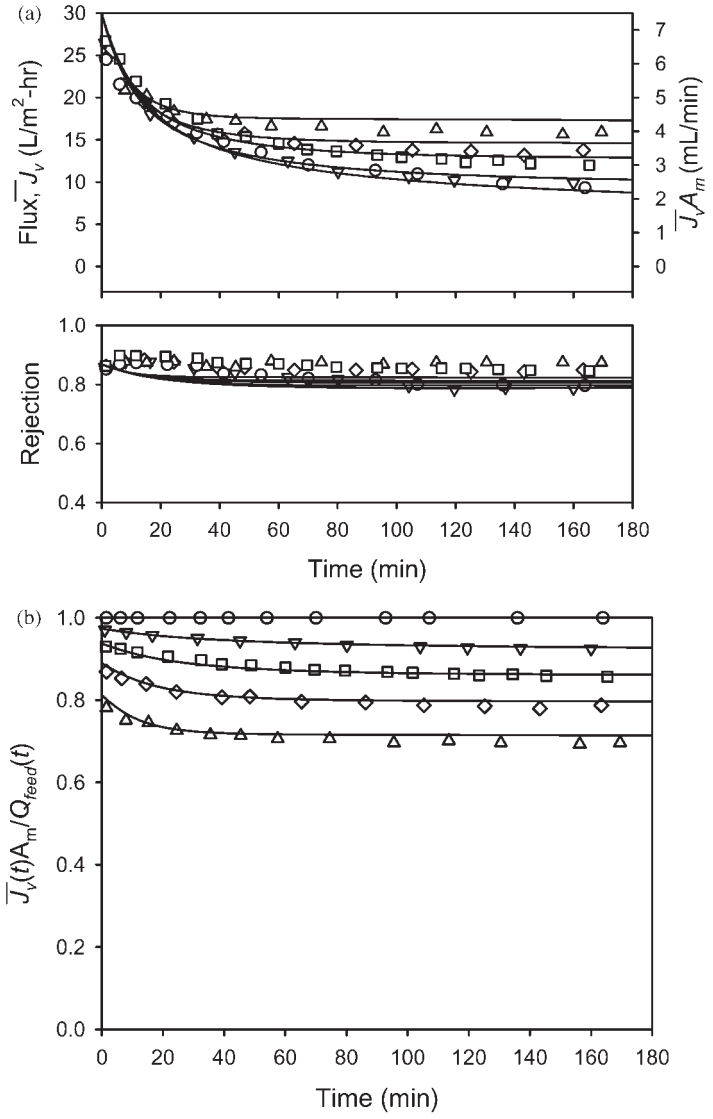

Figure 8. Dependence of permeate flux, total ion rejection, and recovery on time at various concentrate flow rates, for $\Delta P = 1000\,\text{kPa}$, $\omega = 90\,\text{rpm}$ ($\text{Ta}/\text{Ta}_c = 9.75$). Experiments: ○, $Q_{conc} = 0\,\text{mL/min}$; ▽, $Q_{conc} = 0.2\,\text{mL/min}$; □, $Q_{conc} = 0.5\,\text{mL/min}$; ◇, $Q_{conc} = 0.93\,\text{mL/min}$; △, $Q_{conc} = 1.72\,\text{mL/min}$. Model: ——. (a) Permeate flux and total ion rejection and (b) recovery.

MARCEL DEKKER, INC.
270 Madison Avenue, New York, New York 10016

Influence of pH and Feed Concentrations

Wastewater characteristics also play a role in the effectiveness of rotating RO. The simulated space mission wastewater has a pH of 9.5 because of bicarbonate ion formation by urea hydrolysis. Thus, it is important to consider the effect of altering the pH on the flux and rejection. To do this, 2 N sulfuric acid was added to reduce the pH to 6, 7, and 8, in addition to 9.5. Figure 9 shows how pH adjustment affects the flux and rejection. The theoretical model does not account for the effect of pH changes on the membrane permeability, so only a single curve is shown for the model. The permeate flux decreases slightly as the pH is lowered, perhaps because of the increased ion concentration. The rejection increases as the pH is reduced. In both cases, the effects of relatively large changes in pH are minor. These results indicate that pH adjustment would probably not be necessary to optimize rotating RO performance, which is a significant advantage on board a spacecraft where additional treatment of the wastewater to alter the pH is not desirable.

In an actual wastewater treatment application, the composition of wastewater would likely vary. Figure 10 shows how the concentration of

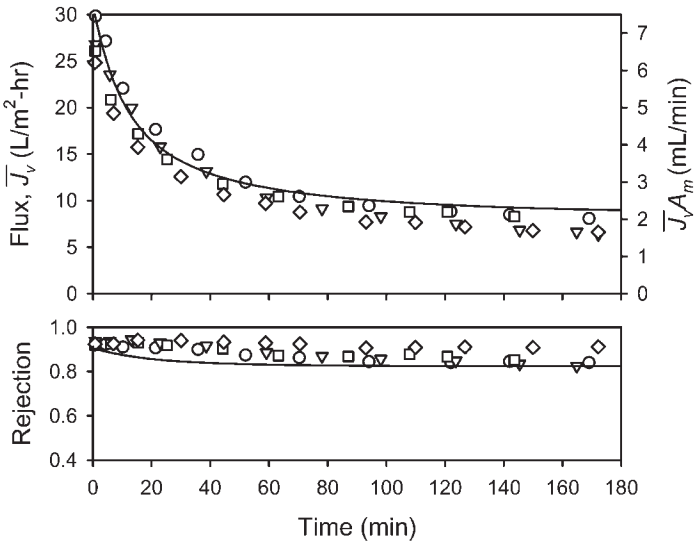

Figure 9. Dependence of permeate flux and total ion rejection on time at different pHs for $\Delta P = 1000$ kPa, $\omega = 90$ rpm, $Q_{conc} = 0.2$ mL/min. Experiments: ○, pH = 9.5 (normal); □, pH = 8; ▽, pH = 7; ◇, pH = 6. Model: ——.

Marcel Dekker, Inc.
270 Madison Avenue, New York, New York 10016

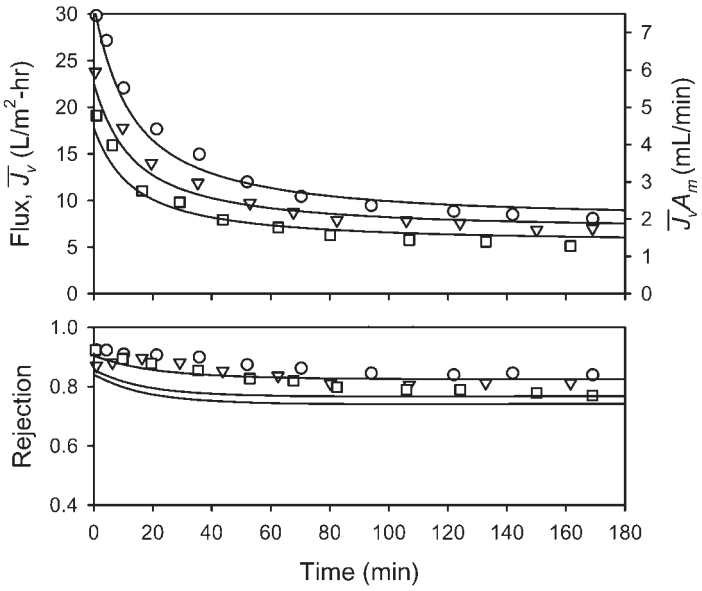

Figure 10. Dependence of permeate flux and total ion rejection on time for different ammonium carbonate concentrations for $\Delta P = 1000\,\text{kPa}$, $\omega = 90\,\text{rpm}$, $Q_{\text{conc}} = 0.2$ mL/min. Experiments: ○, $(NH_4)_2CO_3 = 3429\,\text{mg/L}$ (normal); ▽, $(NH_4)_2CO_3 = 5143$ mg/L; □, $(NH_4)_2CO_3 = 6858\,\text{mg/L}$. Model: ——.

$(NH_4)_2CO_3$ in the wastewater affects the flux and rejection. As the ammonium carbonate concentration doubles from 3429 to 6858 mg/L, the flux decreases by about 40%, most likely because of the increased osmotic pressure. Nevertheless, changes in rejection are small. Thus, rotating RO systems appear to have relatively stable performance even with significant fluctuations in wastewater composition.

Comparison of Model Predictions with Experiments

Finally, we comment on the accuracy of our theoretical solution-diffusion model based on mass conservation and concentration polarization.[19] Figure 11 compares the permeate flux and rejection predicted using the model with the experimental values. Considering the experimental errors inherent in measuring flux at early stages of filtration, the model matches the experimental flux quite well below a flux of $15\,\text{L/m}^2\,\text{hr}$. Above this level, the error is larger but not unreasonable given the wide range of conditions that

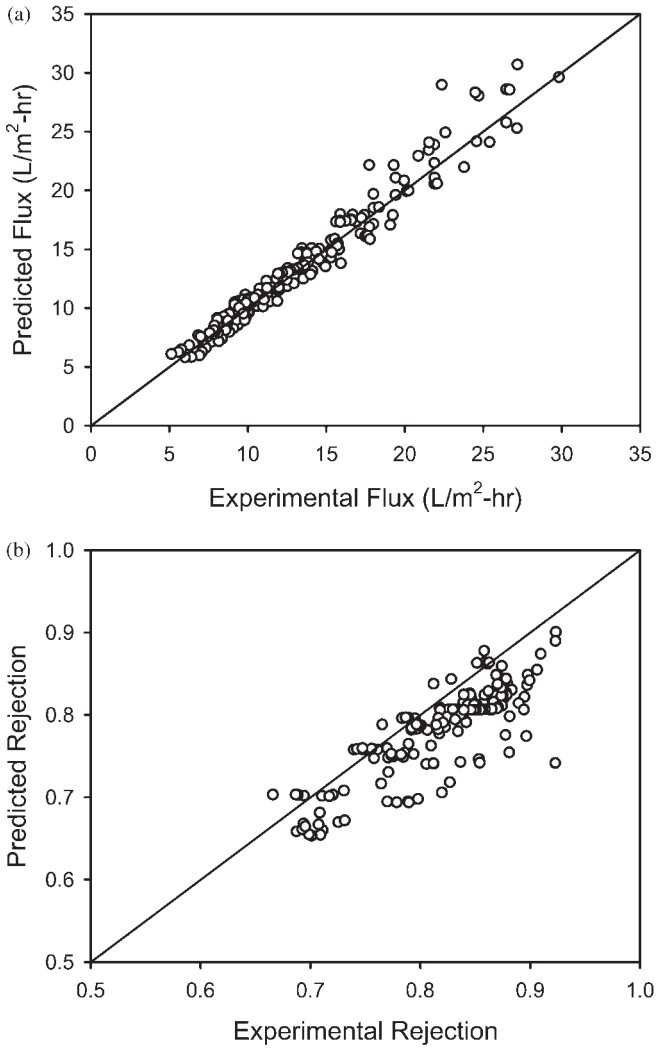

Figure 11. Comparison of model predictions with experiments. Conditions: $\Delta P = 600, 800, 1000$ kPa; $\omega = 7.5, 15, 45, 90, 180$ rpm; $Q_{conc} = 0, 0.2, 0.5, 0.93, 1.75$ mL/min; $(NH_4)_2CO_3 = 3429, 5143, 6858$ mg/L. (a) Flux and (b) total ion rejection.

MARCEL DEKKER, INC.
270 Madison Avenue, New York, New York 10016

were studied and the assumptions in the model. Although there is some scatter in the data, the model typically underpredicts the experimental rejection. This is most likely related to the difficulty in measuring the solute permeability and to the simplicity of the model. However, given that the model underpredicts the rejection, this might be considered a conservative estimate of the rejection.

CONCLUSIONS

The following conclusions can be drawn from this work.

1. The mass transfer increases with increasing rotational speed having a large positive jump at the transition from nonvortical to vortical flow, suggesting that a rotational speed sufficient to generate vortical flow in the annulus is essential to minimize concentration polarization. The mass-transfer coefficients for rotating RO are slightly higher than those for filtration or chemical reactor devices with similar geometries.
2. When treating space mission wastewater, rotating RO shows higher flux and rejection than nonrotating RO. This is because rotating RO significantly decreases concentration polarization.
3. The theoretical model based on mass conservation and the solution-diffusion model with concentration polarization[19] predicts the flux and rejection very well.
4. Increasing the transmembrane pressure and rotational speed improves the flux and rejection in rotating RO. Higher concentrate flow improves the flux, but reduces the recovery.
5. The pH of the wastewater does not affect the flux and rejection significantly. Increased ammonium carbonate concentration in the input wastewater slightly reduces the flux and rejection. However, the changes in flux and rejection due to changes in ammonium carbonate concentration are small enough that rotating RO systems should have relatively stable performance.

ACKNOWLEDGMENT

This work was supported by NASA (grant NAG9-1053), Karen Pickering, contract monitor.

NOTATION

A = constant in Eq. (8)
A_m = membrane area (m^2)
$C_{b,i}$ = concentration of solute i in the bulk solution (mol/m^3)
$C_{f,i}$ = concentration of solute i at feed stream (mol/m^3)
$C_{m,i}$ = concentration of solute i at membrane surface (mol/m^3)
$C_{p,i}$ = concentration of solute i in permeate ($mole/m^3$)
D = diffusion coefficient (m^2/sec)
J_v = permeate flux of water (m/sec)
L_v = water permeability constant ($m^2\,sec/kg$)
$L_{s,i}$ = permeability constant for solute i (m/sec)
P_{loss} = pressure losses (Pa)
ΔP_h = pressure losses due to hydrodynamic effects (Pa)
ΔP = transmembrane pressure (Pa)
Q_{conc} = flow rate of concentrate out of the device (m^3/sec)
Q_{feed} = flow rate of feed solution (m^3/sec)
R = gas constant (J/K)
R_i = rejection for solute i (—)
Sh = Sherwood number ($=2kd/D$) (—)
Sc = Schmidt number ($=\nu/D$) (—)
T = temperature (K)
Ta = Taylor number ($=r_i\omega d/\nu$) (—)
a = exponent for Ta(d/r_i) in Eq. (8)
b = exponent for Sc in Eq. (8)
d = gap width ($=r_o - r_i$) (m)
k_i = mass-transfer constant for solute i (m/sec)
r_i = inner cylinder radius (m)
t = time (sec)
x = axial position (m)
ω = rotational speed (rad/sec)
ν = kinematic viscosity (m^2/sec)
$\Delta\Pi$ = osmotic pressure (Pa)

REFERENCES

1. Dean, R.B. Processes for water reclamation. Waste Manag. Res. **1991**, *9* (5), 425–430.
2. Finger, B.W.; Supra, L.N.; DallBauman, L.; Pickering, K.D. Development and testing of membrane biological wastewater processors. SAE paper **1999**, 1999-01-1947.

MARCEL DEKKER, INC.
270 Madison Avenue, New York, New York 10016

3. Williams, A.D.; Slater, C.S. Recovery of wastewater in microgravity (space) applications using pervaporation processes and volatile rejection membranes. In *Proceedings of the Fifth International Conference on Pervaporation Processes*, Englewood, NJ, USA, 1991.
4. Paul, D.; Ohlrogge, K. Membrane separation processes for clean production. Environ. Prog. **1998**, *17* (3), 137–145.
5. Demboski, D.J.; Benson, J.H.; Rossi, G.E.; Leavitt, N.S.; Mull, M.A. Evolution in U.S. Navy shipboard sewage and graywater programs. In *Proceedings of the ASNE Environmental Symposium on Environmental Stewardship: Ships and Shorelines*, 1997.
6. Ray, R.J.; McCray, S.B.; Newbold, D.D. Small-scale membrane systems for the recovery and purification of water. Sep. Sci. Tech. **1991**, *26* (9), 1155–1176.
7. Lee, S.; Lueptow, R.M. Reverse osmosis filtration for space mission wastewater: membrane properties and operating conditions. J. Membrane Sci. **2001**, *182* (1–2), 77–90.
8. Lee, S.; Lueptow, R.M. Toward a reverse osmosis membrane system for recycling space mission wastewater. Life Support Biosphere Sci. **2001**, *7* (3), 151–161.
9. Wereley, S.T.; Lueptow, R.M. Azimuthal velocity in supercritical circular Couette flow. Exp. Fluids **1994**, *18*, 1–9.
10. Akonour, A.; Lueptow, R.M. Three-dimensional velocity field for non-wavy Taylor Couette flow. Phys. Fluids **2003**, *15* (4), 947–960.
11. Vigo, F.; Uliana, C. Influence of the vorticity at the membrane surface on the performances of the ultrafiltration rotating module. Sep. Sci. Tech. **1986**, *21* (4), 367–381.
12. Belfort, G.; Mikulasek, P.; Pimbley, J.M.; Chung, K.Y. Diagnosis of membrane fouling using a rotating annular filter. 2. Dilute particle suspensions of know particle size. J. Membrane Sci. **1993**, *77* (1), 23–39.
13. Belfort, G.; Pimbley, J.M.; Greiner, A.; Chung, K.Y. Diagnosis of membrane fouling using a rotating annular filter. 1. Cell culture media. J. Membrane Sci. **1993**, *77* (1), 1–22.
14. Lueptow, R.M. *Fluid Mechanics of a Rotating Filter Separator*; American Filtration and Separation Society Northport: AL, USA, 1995.
15. Schwille, J.; Mitra, D.; Lueptow, R.M. Design parameters for rotating cylindrical filtration. J. Membrane Sci. **2002**, *204* (1–2), 53–65.
16. Holeschovsky, U.B.; Cooney, C.L. Quantitative description of ultrafiltration in a rotating filtration device. AIChE J. **1991**, *37* (8), 1219–1226.
17. Hildebrandt, J.R.; Saxton, J.B. *The Use of Taylor Vortices in Protein Processing to Enhance Membrane Filtration Performance*; Bioprocess Engineering Colloquium: ASME Book No. G00422; 1987.

Marcel Dekker, Inc.
270 Madison Avenue, New York, New York 10016

18. Wereley, S.T.; Lueptow, R.M. Inertial particle motion in a Taylor Couette rotating filter. Phys. Fluids **1999**, *11* (2), 325–333.
19. Lee, S.; Lueptow, R.M. Rotating reverse osmosis: a dynamic model for flux and rejection. J. Membrane Sci. **2001**, *192* (1–2), 129–143.
20. Lee, S.; Lueptow, R.M. Experimental verification of a model for rotating reverse osmosis. Desalination **2002**, *146* (1–3), 353–359.
21. Snoeyink, V.L.; Jenkins, D. *Water Chemistry*; John Wiley & Sons, Inc., 1980.
22. Zeman, L.J.; Zydney, A.L. *Microfiltration and Ultrafiltration: Principles and Applications*; Marcel Dekker, Inc.: New York, 1996.
23. Varel, V.H. Use of urease inhibitors to control nitrogen loss from livestock waste. Bioresource Tech. **1997**, *62*, 11–17.
24. APHA; AWWA; WEF. *Standard Methods for the Examination of Water and Wastewater*; Am. Public Health Assoc.: Washington, D.C., 1992.
25. Hach. *Hach Water Analysis Handbook*; Hach Company: Colorado, USA, 1992.
26. Baier, G. *Chemical Engineering*; University of Wisconsin: USA, 1999; Ph.D. Thesis.
27. Mizushina, T. The electrochemical method in transport phenomena. Adv. Heat Transfer **1971**, *7*, 87–100.
28. Coeuret, F.; Legrand, J. Mass transfer at the electrodes of concentric cylindrical reactors combining axial flow and rotation of the inner cylinder. Electrochimica Acta **1981**, *26* (7), 865–872.
29. Kataoka, K.; Doi, H.; Komai, T. Heat/mass transfer in Taylor vortex flow with constant axial flow rates. Int. J. Heat Mass Tran. **1977**, *20* (1), 57–67.
30. Kawase, Y.; Ulbrecht, J.J. Laminar mass transfer between concentric rotating cylinders in the presence of Taylor vortices. Electrochimica Acta **1988**, *33* (2), 199–203.

Received January 2003
Revised August 2003